Supplementary Materials

The present study on the role of mixed fields for spin-flip loss evolved out of our continuing investigations into the collisional processes reported in references [1, 2]. These investigations have revealed that an important fraction of the effects attributed to collisions are in fact attributable to spin-flip losses. In Secs. **??** we provide the interested reader with our current best understanding of the situation. Lastly, we provide in Sec. **??** an algebraic derivation of the loss enhancement factor presented in Eqn. 3 of the main text [**?**].

I. ELECTRIC FIELD INDUCED COLLISIONS

We begin with reference [1] on electric field induced inelastic collisions. The authors identified and investigated the same single particle spin-flip loss enhancement process we discuss in the present work, and an attempt was made at deconvolution from the collisional effect. An appendix of [1] explains this well. Since that time, new observations prompted us to make an even more careful investigation, during which we discovered an important improvement to the mathematics in the appendix of [1].

Relative to the approach taken in the appendix of [1], we make the same simplifying assumptions: loss only occurs in the $\vec{E} \perp \vec{B}$ plane, only the velocity orthogonal to this plane matters, and the population is a thermalized Maxwell-Boltzmann distribution. Our correction relates to the next step, where an integral calculation for the loss rate is performed. In [1] the integration spans the entire 3D spatial distribution, weighted by the frequency of crossing of the center plane and the chance of loss for each crossing:

$$\Gamma_{\rm LZ} = \int_0^\infty 4\pi r^2\, n(r) dr \int_0^\infty n(v_\vartheta) dv_\vartheta \left(\frac{v_\vartheta}{\pi r} P_{\rm hop}(r, v_\vartheta)\right) \quad (1)$$

Here $n(r)$ is the radial distribution function, constrained to satisfy $\int_0^\infty 4\pi r^2 n(r) = 1$, and of the form $n(r) \propto e^{-\mu_B B`r/kT}$. Likewise $n(v_\vartheta)$ is the usual normalized Maxwellian velocity distribution. Implicit in this integration is the simplifying assumption that molecules at a given radius r cross the center plane with a frequency of $v_\vartheta/\pi r$. Though not a bad place to start, this approximation is rather rough given that molecules are certainly not following circular orbits of constant v_ϑ but are in general following some unusual trap motion. Our correction is to perform an integration of flux through the loss plane directly:

$$\Gamma_{\rm LZ} = \int_0^\infty 2\pi r\, n(r) dr \int_0^\infty n(v_z) dv_z \left(v_z P_{\rm hop}(r, v_z)\right) \quad (2)$$

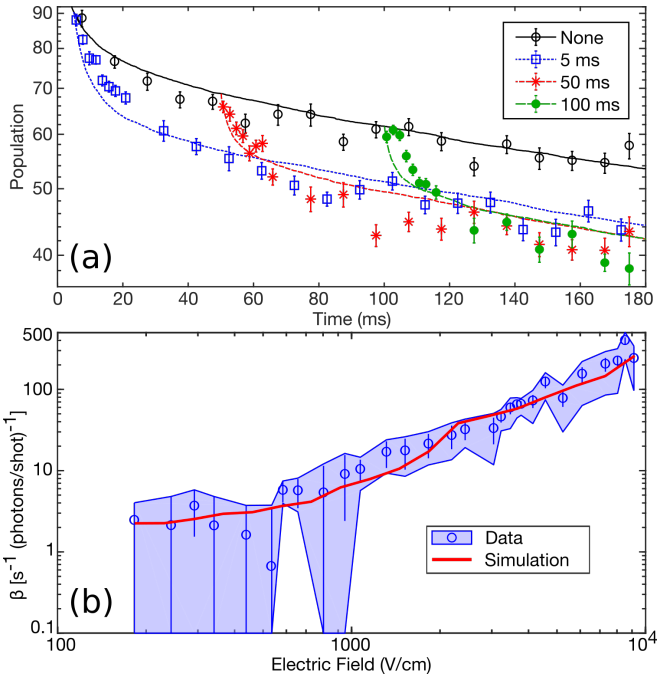

FIG. 1. Experimental electric field induced loss data with an attempted overlap to spin-flip loss simulations. The case of no electric field (black, solid) is compared to electric fields of in 3 kV/cm turned on after a wait time indicated in the legend. (b) Two body fits from [1] to experimental data like that in (a) but at various electric fields. The blue data points and shaded region are repeated from Fig. 3 of [1], where the shading indicates the variation that would be brought about by changes in the single particle effect by a factor of two in either direction. Even though we discover a factor of only three, the spin flip loss simulation (thick red solid line) matches the data within errorbars.

Here the same distributions are used, but the spatial distribution is integrated over the central plane only, hence the $2\pi r$ Jacobean, and the hopping probability is multiplied by the velocity v_z to give a flux. The coordinates z and ϑ are mathematically equivalent in the central plane, but z is more appropriate given that integration is no longer spanning the ϑ direction. This flux integral gives the desired loss rate without any approximations about molecule orbits or plane-crossing frequency. Although the two integrals differ significantly in their conception, mathematically the changes to the integrand and the Jacobean reduce to precisely an overall scaling factor of π.

The influence of this on the deconvolution procedure relates to the details of the two-body fitting routine. One plus two body fits were performed to various decay trap curves, with the one body component fixed to the value expected due to vacuum scattering and spin-flip loss. An example of such decay curves is shown in Fig. 1(a), where Electric field is turned on suddenly after various hold

times. With the stronger spin-flip loss, it is no longer appropriate to assume this loss will be present in the data as a pure one-body decay. Rather, only those molecules whose orbits regularly intersect the loss region are lost, after which thermalization would be required to repopulate the loss prone regions of phase space. If thermalization is slow, spin-flip loss can have a rate that decreases over time, producing a time dependence of population like that of a two-body effect. Even though the possibility of a factor of two error in the calculated magnitude of spin-flip loss was considered in [1] (Fig. 1(b), shaded region), the possibility of its influencing the data in a non-single-particle manner was not considered.

We can perform single particle simulations of spin-flip loss to investigate this, and we obtain curves such as shown above the time dependent experiment data points in Fig. 1(a). We can even perform a two body fitting procedure like the one used in [1] to the single particle spin-flip loss simulation traces, see Fig. 1(b). The results suggest that the effect attributed to two-body collisions could be largely explained by spin-flip losses. Still, there are notable differences, such as in the initial rate of the decays in fig. 1(a), which is faster in simulation than in experiment, and in the long time magnitude of the loss, which is maybe 10% larger in experiment than simulation. One avenue to try and be more quantitative would be to incorporate collisions in the simulation and see what collision rates yield the best agreement. Unfortunately there are many challenges in the quantitative application of these simulations, such as uncertainty regarding the initial distribution and the existence of various partially trapped substates. We think the best path forward is to perform future collisional studies with the single-particle effect removed [**?**].

II. EVAPORATION

With regard to [2], the present study is one of a number of important modifications to our understanding that have come up in recent years. It was originally thought that the measured spatial distribution in the trap was consistent with the buildup of a cold population in a region that was insensitive to our spectroscopy. This was supported by the direct optical detection of this population and by the goodness of fits performed under the hypothesis. Regarding the fits, an important correction has been discovered and is discussed in [4], where a thorough investigation of hyperfine shifts and external field effects was performed for OH. This correction results in a 15% increase in the magnetic dipole moment used to interpret spectroscopy, and thus to the magnetic field at a particular microwave frequency. The data show a sudden suppression below 480 G, consistent with the hypothesis of a suppressed population only if this is the location of a certain avoided crossing, but with the magnetic dipole moment correction the crossing is actually located closer to 400 G. Without this, the fits used to calculate temperature under the suppression hypothesis are no longer trustworthy. Without the suppression hypothesis, the temperatures fit in Fig. 3 of [2] are not reliable.

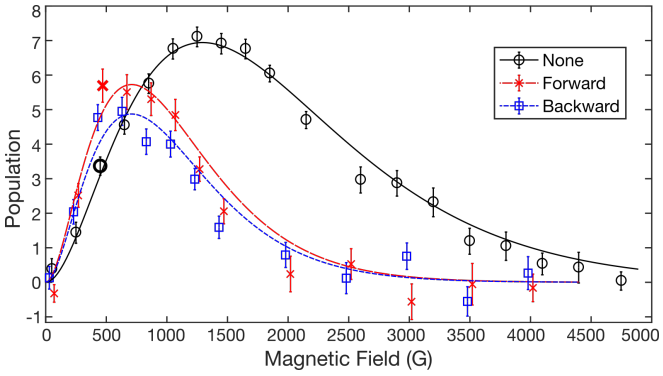

FIG. 2. Normalized spectra are performed under three conditions: one with no evaporation (black circles), one with an exponential RF evaporation ramp over 170 ms (red x's), and a third with this ramp applied in a time reversed manner (blue squares). Solid lines are fits to Maxwell-Boltzmann distributions with temperatures of 51 ± 2 in the case of no evaporation (black), and 30 ± 3 for both forward (red, long dashes) and backward (blue, short dashes) evaporations. The forward evaporation achieves a clear density enhancement in the vicinity of 500 G, where the line markers are bolded.

This is the same conclusion supported by the enhanced magnitude of spin-flip losses we are reporting. At the temperatures fitted to those spectra, the spin-flip loss caused by the electric field used during evaporation are large enough to significantly influence the population, see Tab. 1 in [**?**]. Nonetheless, without fitting temperatures, it is still possible to use normalized spectra to look for enhancements in density caused by the evaporation. The normalization simply rescales the trace so that the area beneath adds up to the observed total population by laser induced fluorescence. Without it, spectroscopies of smaller populations yield distributions with enclosed areas that are decreased much more than the actual population. All of the evaporation traces in Fig. 3 of [2] show density enhancements in the region near 500 G, but a further correction changes this. By more carefully investigating the usage of microwave chirp rates and powers, we confirmed that what was previously interpreted as a frequency offset was in fact an "oort cloud" persisting at larger fields [6]. After accounting for this, only Fig. 3c of [2] shows an enhancement, but it does so very clearly and repeatably as in Fig. 2.

We have also developed a few more sensitive tools to look for collisional or evaporative effects. One is the ability to reduce population without perturbing phase space distribution, mentioned and used to look for collisions in [**?**]. This is non-trivial, and many possible techniques have key drawbacks. For example it is not possible to change the discharge yield of OH in our supersonic expansion without also influencing the temperature of the initial distribution, which is effected by the

discharge. We opt for the application of microwaves during deceleration to couple weak and strong field seeking states at low magnitudes of electric fields experienced by all molecules when flying through a de-energized stage just after switching. The microwaves are applied via microwave horn and have a long wavelength relative to the cloud, so that microwave power variations across the cloud are not relevant. The microwaves are applied early during deceleration, so that the molecules have many stages of deceleration and the process of trap-loading left to remix any asymmetries in the removal process. It is difficult to experimentally verify that the phase space distribution function is truly unaffected in all six dimensions, but in at least one dimension, the time of flight profile of slowed molecules after deceleration, the distribution is unaffected even by tenfold reductions using this technique. Unfortunately we have only recently developed this capability and cannot back-apply it to the experiments in [2].

Another tool is to compare the populations under two related conditions- the first a normal evaporation sequence and the second an evaporation with time-reversed microwave frequency. In other words, the cut goes backwards from deep to shallow. This comparison subjects all molecules to the same integrated microwave power, and thus the two conditions should be equivalent in a situation with only single particle effects. One possible exception could be the existence of very slow single particle transfers to other trapped substates which could hide from the microwaves or interact with them differently, but we find no clear evidence for this. With evaporative effects, the normal condition ought to perform better, though perhaps not very significantly if the sequence is not well optimized. This we have performed in the original system, and we consistently observe higher final numbers from the forward sequence, at the 5% level, see Fig. 2.

In conclusion, the roles of collisional effects in Refs. [1, 2] are reduced by spin-flip losses and other modifications to our understanding. Despite the effect of spin-flip losses and some other discoveries, spectroscopic comparisons and evaporation subtractions still point to an evaporative effect. The development of various more sensitive tools has us poised to more unambiguously identify any future collisional effects in our next generation system.

III. SCALING LAW DERIVATION

Here we derive the loss enhancement scaling law presented in Eqn. 3 of the main text [**?**], and repeated here:

$$\eta = \left(\frac{d_{\rm eff}E}{\sqrt{\kappa\Delta}}\right)^{8/3}. \tag{3}$$

The key idea is to compare the areas of the contour surfaces of energy κ which sets the energy below which spin-flips can occur. There is no exact energy scale for which a molecule is guaranteed to hop, but rather their velocity and direction contribute to the Landau-Zener probability (Eqn. 2, Ref. [**?**]). For the purposes of a scaling law, the average thermal velocity v_T normal to the surface can be used, and a probability threshold of $P > 1/e$. These assumptions allow us to define:

$$\kappa = \sqrt{\hbar\dot{G}} = \sqrt{2\hbar v_T B'}, \tag{4}$$

where G is the energy gap between the trapped state and its spin flip partner, and B' is the trap gradient.

One complication is that in a quadrupole trap there is a weak and a strong axis, so that B' varies by as much as a factor of two in different directions. Once a sufficient electric field is applied, the gradient in the two directions within the loss plane becomes negligible, (Eqn. 1, Ref. [**?**]) and only the gradient normal to the loss plane matters. In the case of electric field applied between the faces of permanent magnets used to create a magnetic quadrupole trap, the loss plane is normal to the strong axis of the trap, so we use B' to refer to this strong axis throughout. Before application of electric field, the κ valued energy contour is an oblate ellipsoid of long radius $r_0 = 2\kappa/\mu_{\rm eff}B'$. It's area is then $2\pi \cdot 1.38 r_0^2$, where the prefactor comes from the specific $2:1$ aspect ratio of the ellipsoid.

Now when electric field is applied, the energy gap near the trap zero takes the following functional form:

$$G(r,z) = B'|z| + (\frac{1}{2}\mu_{\rm eff}B'r)^3\frac{\Delta^2}{(d_{\rm eff}E)^4} + \mathcal{O}(z^2, r^4). \tag{5}$$

Here we use r to denote the in-loss-plane coordinate and z to denote distance away from the loss plane, along the strong axis of the trap. This is essentially Eqn. 1 of Ref. [**?**] with an explicit coordinate system. Now we compute the area of the surface $G = \kappa$. The radial extent of the surface can be solved by inverting $\kappa = G(r, 0)$:

$$r_E = \frac{1}{\mu_{\rm eff}B'}\sqrt[3]{\frac{8\kappa(d_{\rm eff}E)^4}{\Delta^2}} \tag{6}$$

The axial extent, $z = \kappa/B'$, is miniscule by comparison, so the area of the contour is just $2\pi r_E^2$. Putting the pieces together, the loss enhancement is then $\eta = (r_E/r_0)^2$ so that $\mu_{\rm eff}B'$ cancels and so

$$\eta = \frac{1}{2\kappa}\sqrt[3]{\frac{8\kappa(d_{\rm eff}E)^4}{\Delta^2}} = \left(\frac{d_{\rm eff}E}{\sqrt{\kappa\Delta}}\right)^{8/3}. \tag{7}$$

[1] B. K. Stuhl, M. Yeo, M. T. Hummon, and J. Ye, Molecular Physics **111**, 1798 (2013).
[2] B. K. Stuhl, M. T. Hummon, M. Yeo, G. Quéméner, J. L. Bohn, and J. Ye, Nature **492**, 396 (2012).
[3] See the main text.
[4] K. Maeda, M. L. Wall, and L. D. Carr, New Journal of Physics **17**, 45014 (2015).
[5] See the main text.
[6] M. Inguscio, S. Stringari, C. E. Wieman, and S. italiana di Fisica., in *Varenna on Lake Como, Villa Monastero, 7-17 July 1998* (IOS Press, Amsterdam; Washington, DC, 1999).